Electrochimica Acta 56 (2011) 9838–9845

Contents lists available at SciVerse ScienceDirect

Electrochimica Acta

journal homepage: www.elsevier.com/locate/electacta

# Flexible electrodes based on polypyrrole/manganese dioxide/polypropylene fibrous membrane composite for supercapacitor

Ming Jin, Gaoyi Han*, Yunzhen Chang, Hua Zhao, Huanyu Zhang

*Institute of Molecular Science, Key Laboratory of Chemical Biology and Molecular Engineering of Education Ministry, Shanxi University, Taiyuan 030006 PR China*

ARTICLE INFO

*Article history:*
Received 3 April 2011
Received in revised form 2 August 2011
Accepted 17 August 2011
Available online 30 August 2011

*Keywords:*
Conducting polymer
Polypyrrole
$MnO_2$
Supercapacitor, Polypropylene

ABSTRACT

The composites of polypyrrole/manganese dioxide/polypropylene fibrous films (PPy/$MnO_2$/PPF) have been prepared in situ through chemical oxidation polymerization by using the mixture of $FeCl_3 \cdot 6H_2O$ and $MnO_2$ adsorbed on PPF as oxidant in the atmosphere of pyrrole vapor at room temperature. The morphologies and structures of the composites are investigated by using scanning electron microscope and X-ray diffraction spectroscopy. The properties of the capacitor cells assembled by the composites of PPy/$MnO_2$/PPF are evaluated by cyclic voltammetry, galvanostatic charge/discharge and electrochemical impedance spectroscopy methods. The results reveal that the morphologies, conductivities and capacitance performance of the composites are influenced strongly by the content of $MnO_2$ in the solution of oxidant. The capacitors assembled by PPy/$MnO_2$/PPF exhibit the property of quick charge/discharge, and the highest specific capacitance of about 110 F $g^{-1}$ is obtained when the PPy/$MnO_2$ content in the composite is about 17.4%.



## 1. Introduction

Recently, much attention has focused on the electrochemical capacitors which will be developed as novel energy-storage devices owing to their high power density, long life cycles, and high efficiency [1–9]. Generally, two types of supercapacitors can be constructed based on the kind of the electrode materials: one is the electrical double-layer capacitor which utilizes mainly the separation of the electronic and ionic charges at the interface between electrode materials and the electrolyte solution [10,11], the other is the pseudo-capacitor based on the Faradaic redox reactions occurring within the active materials of electrodes [12,13]. Carbon materials with high surface area such as carbon nanotubes, active carbon and graphene have been widely investigated for double-layer capacitor. As an ideal candidate for pseudo-capacitor electrodes, polypyrrole (PPy) has attracted considerable attention [14–16] owing to its high electrical conductivity, the excellent stability for redox and the benign property to environment [17–20]. To date, various methods of polymerization including polymerization in solution [21], in vapor phase [16,19,22] and under supercritical conditions [23] have been applied to prepare PPy with various microstructures.

Recently, many attempts have been made in the energy storage devices consisting of entire nonmetal components in order to fit the development of flexible and wearable electronics. The flexible electrodes based on the conducting polymer are usually fabricated until now by depositing conducting polymer on the nonmetal flexible substrates. The composite can combine the properties of the constituents and make it possible to overcome the drawbacks of the individual substances [24–27]. For example, the electrodes fabricated by depositing PPy on the carbon fibers, celluloid and polysaccharide fibers have been investigated as the material of capacitors [28–35]. On the other hand, it is well known that electrochemically active metal oxide such as $MnO_2$, one of the most stable manganese oxides, exhibits excellent physical and chemical properties under ambient condition besides the rich polymorphism and structural variety and has been widely used in the fields of catalysis, biosensor and energy storage [36–40]. It is expected that the excellent properties may come into being when the properties of PPy and $MnO_2$ are combined together.

In present work, the flexible composites of PPy/$MnO_2$/PPF will be conveniently prepared through a simple route of polymerization in situ vapor phase. During the process the electrochemically active material of PPy/$MnO_2$ will combine with the substrate of PPF which exhibits good mechanical property, flexibility, chemical resistance and relatively high surface-to-mass ratio. It is expected that the composites will exhibit the flexibility as well as the porosity

* Corresponding author. Tel.: +86 351 7010699; fax: +86 351 7016358.
*E-mail address:* han_gaoyis@sxu.edu.cn (G. Han).

0013-4686/$ – see front matter © 2011 Elsevier Ltd. All rights reserved.
doi:10.1016/j.electacta.2011.08.079

and fit the characteristics of electrodes applied in electrochemical capacitor.

## 2. Experimental

### 2.1. Reagents and materials

Acetonitrile, anhydrous ethanol, KCl, $KMnO_4$, $MnSO_4{\cdot}H_2O$ and $FeCl_3{\cdot}6H_2O$ were analytical grade and used without further purification. Pyrrole was distilled under reduced pressure prior to use and stored at a temperature less than 5 °C. The PPF formed by polypropylene micro-fibers with many cumulate pores and a thickness of about 450 μm was purchased from Cullender Factory of Guodian. The nano-sized $MnO_2$ were synthesized under hydrothermal condition according previous method [41]. In a typical procedure, equal volume of $KMnO_4$ (0.05 mol $L^{-1}$) and $MnSO_4{\cdot}H_2O$ (0.075 mol $L^{-1}$) solutions were mixed and stirred strongly until a homogeneous solution was formed. Then the mixture was transferred into a Teflon-lined autoclave with a stainless steel shell, subsequently, the autoclave was heated and kept at 140 °C for 15 h. After cooling, the product was collected and washed with distilled water and anhydrous ethanol several times, and dried under vacuum at 60 °C.

### 2.2. Preparation of the flexible composites of PPy/$MnO_2$/PPF

The flexible PPy/$MnO_2$/PPF composites were prepared by using $FeCl_3{\cdot}6H_2O$ dissolved in acetonitrile containing various amount of $MnO_2$ as oxidant to react with the pyrrole vapor in an airtight vessel at room temperature. In a typical process, the PPF films were soaked in the solution of $FeCl_3{\cdot}6H_2O$ (360 mg $mL^{-1}$) containing various amounts of $MnO_2$ for 15 min under ultrasonic condition. After the excess solution was eliminated by a filter paper, the PPF films containing the mixture of $FeCl_3{\cdot}6H_2O$ and $MnO_2$ were suspended in a sealed vessel where the oxidant reacted with the pyrrole vapor at room temperature for 4 h. Finally, the composite of PPy/$MnO_2$/PPF was dried in vacuum at room temperature for 12 h after the impurity being removed through washing with ethanol several times. The content of PPy/$MnO_2$ in the composites was determined by the weight of the composites and PPF. The PPy/$MnO_2$/PPF prepared by using $FeCl_3{\cdot}6H_2O$ acetonitrile solution containing 3, 5 and 6 mg $mL^{-1}$ $MnO_2$ as oxidant were named as composites a, b and c, respectively. The content of PPy/$MnO_2$ in the composites was measured to be about 10.0, 17.4 and 23.4% in the composites a, b and c, respectively.

### 2.3. Characterization

The morphologies of the PPy/$MnO_2$/PPF were observed on a scanning electron microscope (JEOL SEM 6701F) and the X-ray diffraction (XRD) patterns were recorded on a Bruker D8 Advance X-ray diffractometer (Cu Ka) in the 2$\theta$ range of 10–80°. The electrical conductivities were measured by using the standard four-probe technique. The capacitor cells were assembled by using two same pieces of PPy/$MnO_2$/PPF composite (one oxidized and the other reduced) as the two electrodes, and a piece of filter paper soaked with 1.0 mol $L^{-1}$ KCl was used to separate the two pieces of PPy/$MnO_2$/PPF (Fig. 2A). Two platinum foils contacted with the composites were used as the current collectors while two pieces of polyvinylchloride plates were utilized to coat and stabilize the cell. The electrochemical measurements were carried out on a CHI 660 C electrochemical station by using double-electrode technique. The measurements of cyclic voltammetry (CV) were performed in a potential range of −0.5 to 0.5 at different scan rates. Galvanostatic charge/discharge curves were recorded at varying current densities with the cutoff voltage of −0.5 and 0.5 V. The electrochemical impedance spectra (EIS) were recorded at open-circuit potential in the frequency ranged from 100,000 to 0.01 Hz with ac-voltage amplitude of 5 mV.

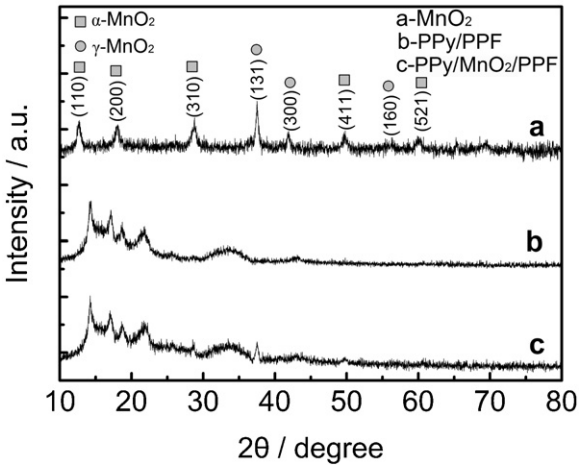


**Fig. 1.** The XRD patterns of $MnO_2$ nanoparticles as prepared (a), PPy/PPF (b) and PPy/$MnO_2$/PPF containing 32.7% PPy/$MnO_2$ (c).

## 3. Results and discussion

### 3.1. The characteristic of the XRD patterns

As displayed in Fig. 1, the XRD pattern of the nano-sized $MnO_2$ prepared by hydrothermal method at 140 °C (Fig. 1a) shows two sets of diffraction peaks which can be assigned to tetragonal α-$MnO_2$ (JCPDS No. 44-0141) and orthorhombic γ-$MnO_2$ (JCPDS No. 14-0644), respectively [42]. The average diameter of α-$MnO_2$ is determined to be about 4.5 nm according to the Scherrer formula ($d = 0.89\lambda/B\cos\theta$). The composite of PPy/PPF shows a broad peak centered at 33.5° (Fig. 1b), which is corresponding to the closest distance of the planar aromatic rings in the PPy with amorphous structure [43]. At the same time, the peaks located at 15–25° can be assigned to the diffraction resulted from polypropylene [44]. The composite of PPy/$MnO_2$/PPF shows the diffraction peaks corresponding to $MnO_2$ at 28.8, 37.5 and 49.8° besides the diffraction peaks related to PPy and polypropylene (Fig. 1c), indicating that the composite has been formed.

### 3.2. Conductivity and morphology

Fig. 2A shows the structural illustration of the capacitor cell assembled by the composites. Fig. 2B shows the plots of the content of PPy/$MnO_2$ in the composites and the conductivities of the composites versus the amount of $MnO_2$ in the oxidant solution. It is found that the content of PPy/$MnO_2$ increases with the increment of $MnO_2$ in the acetonitrile solution of $FeCl_3{\cdot}6H_2O$, for example, the content of PPy/$MnO_2$ in the composites is 3.4, 10.0, 17.4, 23.4 and 32.7% when the content of $MnO_2$ in oxidant solution is 1.0, 3.0, 5.0, 6.0 and 7.0 mg $ml^{-1}$, respectively. The reason may be that more $MnO_2$ particles are favorable for the adsorption of the oxidant solution on the fibers. It is also found that the conductivity of the composites increases with the increment of $MnO_2$ in the oxidant solution. Furthermore, the conductivity of the composite is almost kept constant after reaching the maximum of about 1.02 S $cm^{-1}$ when the content of $MnO_2$ in oxidant solution is about 7 mg $ml^{-1}$.

From Fig. 2C, it can be found that the composite containing 23.4% PPy/$MnO_2$ can be bent easily. The flexibility of the composites is fairly good when the content of PPy/$MnO_2$ is no more than 23.0%. However, the flexibility of the composite containing 32.7%

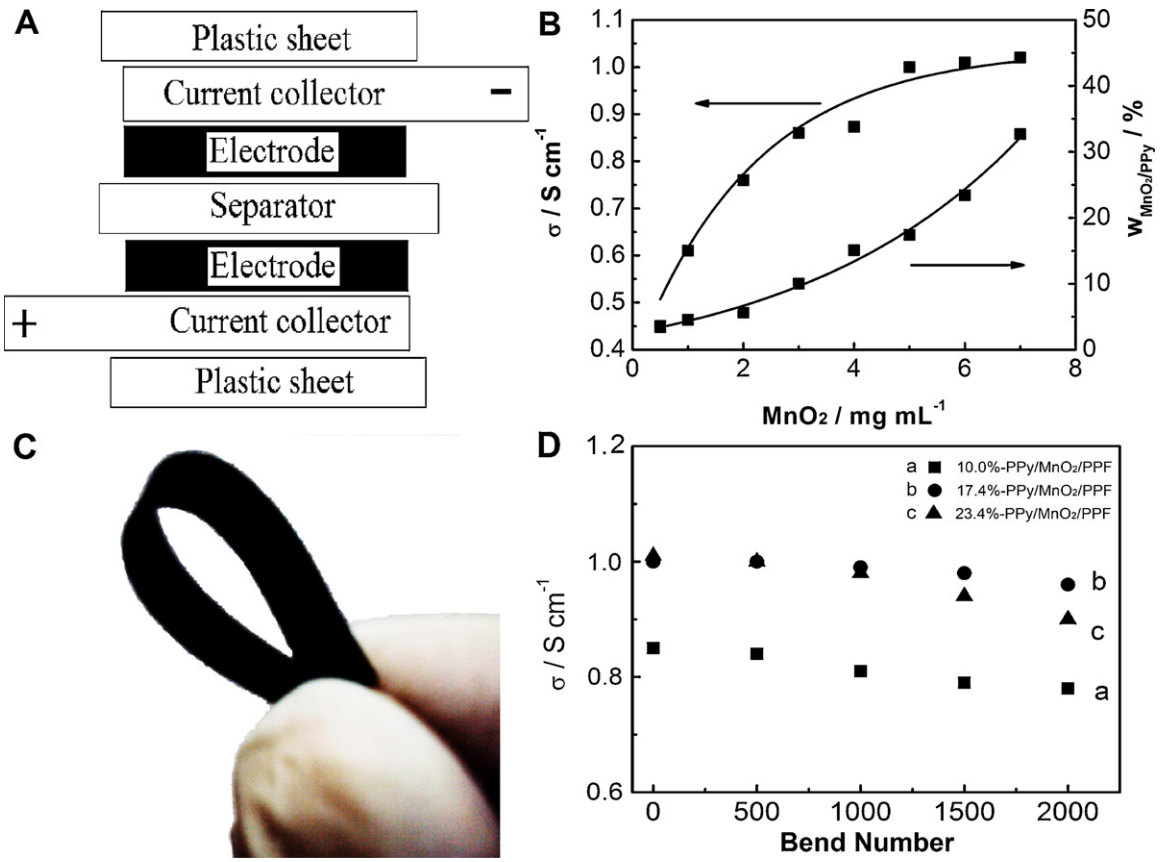


**Fig. 2.** Schematic image of the capacitor cell (A) and the relationship between the content of PPy/$MnO_2$ and conductivities and the amount of $MnO_2$ in $FeCl_3{\cdot}6H_2O$ solution (B). Left: conductivity, right: percent ration of PPy/$MnO_2$ in the composites, the photograph of the composite containing 23.4% PPy/$MnO_2$ under bent condition (C) and the relationships between the conductivities of the composites and the bend numbers (D).

PPy/$MnO_2$ becomes bad and some PPy/$MnO_2$ particles flake off the composite when the film is bent. Furthermore, the conductivities of the composite of a, b and c are also measured by four-probe technique after certain times of bend. The relationships between the conductivities of the composites and the bend numbers are shown in Fig. 2D, from which it can be seen that the conductivities of the composites decrease slightly with the increment of the bent times, and that the decline of the conductivity of composite b exhibits a more gentler trend than that of composites of a and c, indicating that composite b will exhibit better property.

The SEM image of the PPF is shown in Fig. 3A, from which it can be seen that the surface of the fibers is smooth and the diameter of

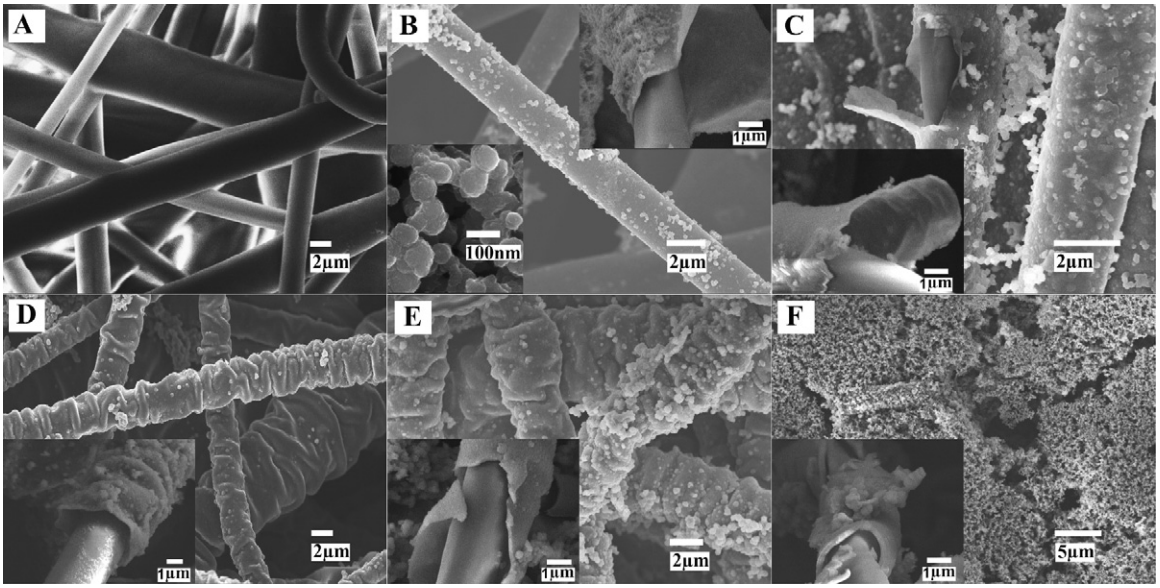


**Fig. 3.** SEM images of (A) pristine PPF film, and the SEM images of composite PPy/$MnO_2$/PPF containing different PPy/$MnO_2$ 3.4% (B), 10.0% (C), 17.4% (D), 23.4% (E) and 32.7% (F), the inserted SEM image in (B)–(F) are recorded for the thickness of the PPy layer.

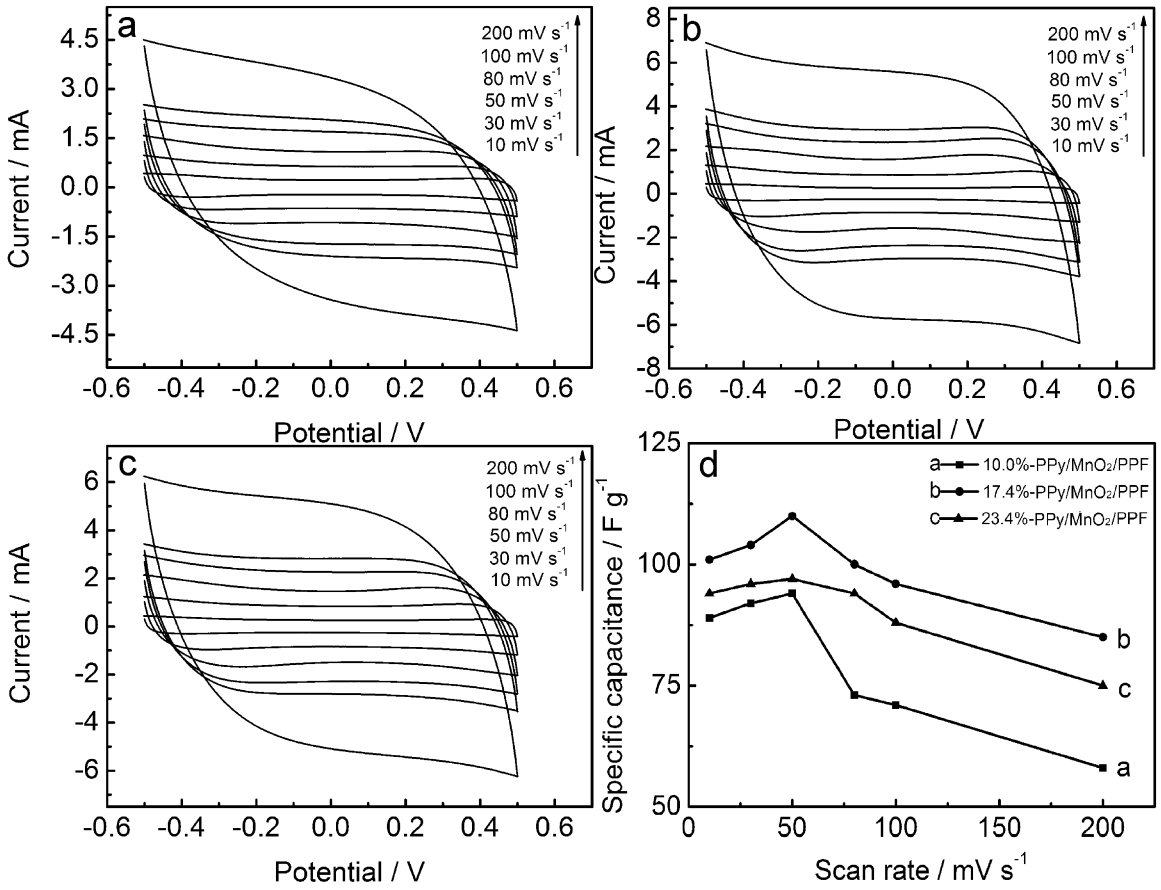


**Fig. 4.** CV behaviors of the capacitor cells assembled by PPy/$MnO_2$/PPF composites a (A), b (B) and c (C), and the plots of specific capacitances of the capacitor cell prepared by PPy/$MnO_2$/PPF composites a, b and c (D).

the fibers ranges from 3 to 6 μm except some fibers with a diameter larger than 10 μm, and that the cumulate pores ranged from several hundred nanometers to several micrometers are observed on the surface of PPF. However, the morphologies of PPy/$MnO_2$/PPF (Fig. 3B–F) are obviously different from that of PPF, for example, the surface of the fibers becomes coarse because the composite of PPy/$MnO_2$ has formed on the surface of polypropylene fibers. Furthermore, the morphologies of PPy/$MnO_2$/PPF change with the increment of the $MnO_2$ content in oxidant solution. It is noted that some particles are dispersed on the surface of polypropylene fibers coated with a layer of PPy/$MnO_2$ (Fig. 3B and C) when the content of $MnO_2$ in oxidant solution is as low as 0.5 and 3.0 mg $ml^{-1}$. As shown in Fig. 3D and E, the wrinkly and coarse layers of composite have appeared on the surface of polypropylene fibers when the $MnO_2$ content increases to 5.0 mg $mL^{-1}$, and the PPy/$MnO_2$ particles are believed to be present not only on the surface of the composite but also in the interior of the composite. Finally, the pores dispersed on the surface have been filled with the formed product (Fig. 3F) when the content of the $MnO_2$ increases to 7.0 mg $mL^{-1}$ or ever further in the oxidant solution. It is interesting to find from the inserted

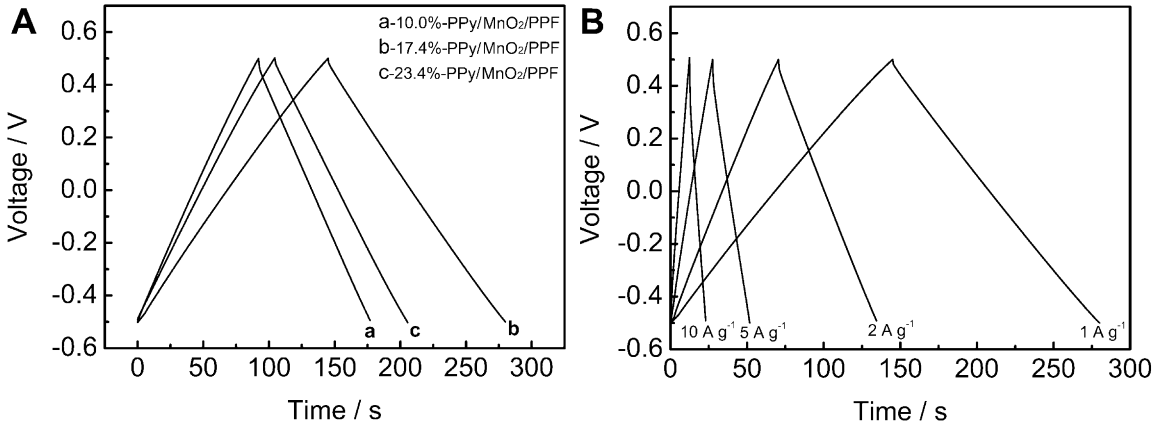


**Fig. 5.** Charge/discharge curves of PPy/$MnO_2$/PPF composite containing different amounts of PPy/$MnO_2$ at current density of 1.0 A $g^{-1}$ (A) and charge/discharge curves of the cell assembled by PPy/$MnO_2$/PPF composite b at various current densities (B).

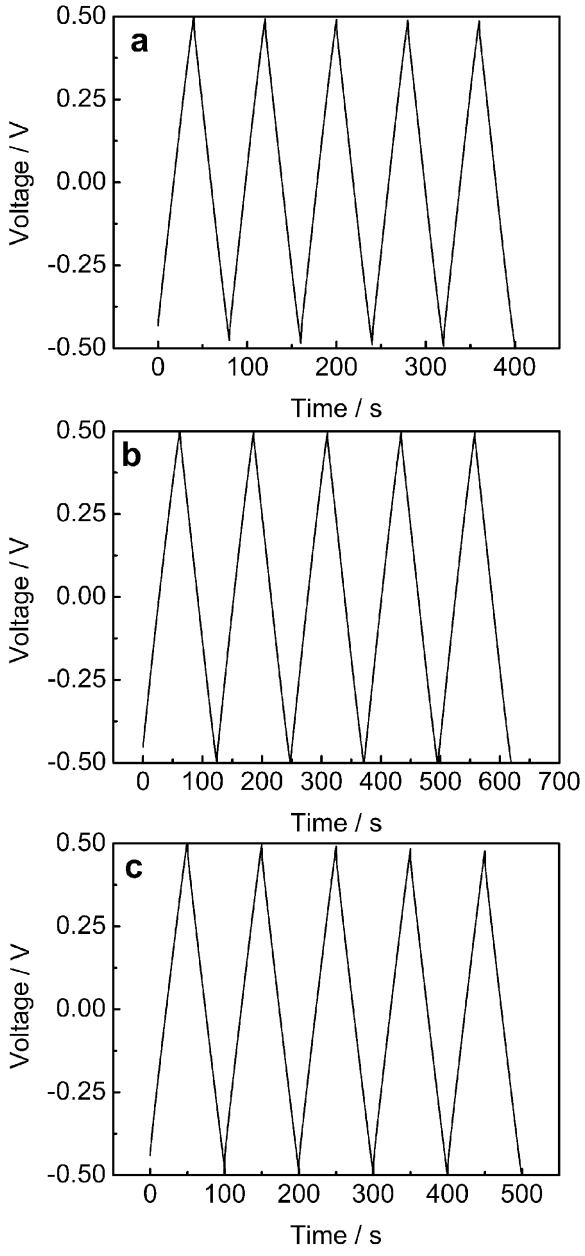


**Fig. 6.** Charge/discharge cycling curves of the cells prepared by PPy/$MnO_2$/PPF composites a (A), b (B) and c (C) at current density of 2.0 A $g^{-1}$.

SEM images in Fig. 3B–F that the PPy layer does not closely contact the PP fibers, and there is some spacing between the PPy layer and surface of PP fiber. The thickness of the PPy layer in the composites increases slightly with the increment of the content of PPy/$MnO_2$, for example, the thickness of PPy is about 99, 137, 162, 170 and 199 nm when the content of PPy/$MnO_2$ is about 3.4, 10.0, 17.4, 23.4 and 32.7% in the composites.

In low content of $MnO_2$, the formed PPy/$MnO_2$ particles and PPy enwrap the PP fibers and the conductivity increases with the increment of the $MnO_2$ in the oxidant solution because of the increment of conducting material; yet, the thickness of the composite films increases and the resistance decreases with the increment of $MnO_2$ in the $FeCl_3{\cdot}6H_2O$ solution, so the conductivity almost remains changeless when reaching the maximum.

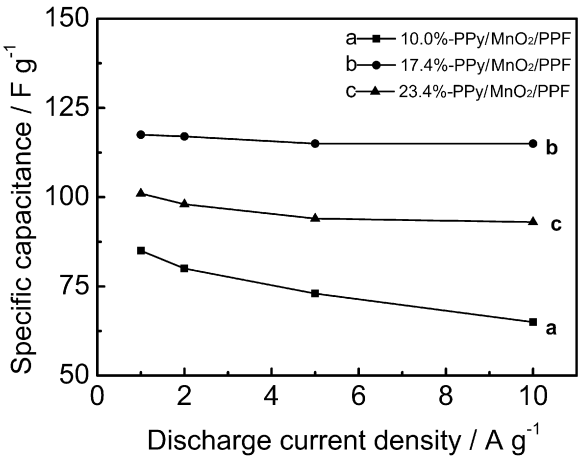


**Fig. 7.** Discharge capacitance of the capacitors assembled by PPy/$MnO_2$/PPF composite at various discharge current densities.

### 3.3. Electrochemical properties of the capacitor cells assembled by PPy/$MnO_2$/PPF

The curves of CV for capacitor cells assembled by the PPy/$MnO_2$/PPF films are recorded at different scan rates and shown in Fig. 4A–C. It can be found that the curves at different scan rates do not show redox peaks corresponding to either PPy or $MnO_2$ in the whole voltage range during the both positive and negative sweeps, indicating that the electrode is charged and discharged at a pseudo-constant rate over the whole CV process. The shapes of the curves are rectangular-like with the almost symmetric *I*–*E* responses when the scan rates are lower than 100 mV $s^{-1}$, which are corresponding to the rapid current response on voltage reversal at each end potential and accord to the ideal capacitive behavior. It can be also found that the curves of CV shown in Fig. 4B display more rectangular-like than that shown in Fig. 4A and C, which illustrates the composite b exhibits better property of capacitor than composites a and c. Furthermore, the capacitor cells assembled by composite b remain rectangular-like CV curves while the cells prepared by the composites a and c cannot keep rectangular-like curves when the scan rate increases to 200 mV $s^{-1}$. The above results indicate that rapid charge/discharge reaction can occur in composite b because it exhibits the optimal conductivity and structures modified by $MnO_2$, which is favorable for the motion of counter ion in the polymer matrix. It is well known that the redox reactions occurring on the PPy mainly attend by the doping-undoping counter ion ($Cl^-$) in the matrix of the polymer [26], and the ions diffused from the electrolyte have access to almost all available spaces at low scanning rates, leading to a complete insertion reaction. However, with the increase of the scanning rates, the effective interaction between the matrix and the electrolyte will reduce greatly, so the deviation from rectangularity of the CV becomes obvious.

In order to analyze the variation of capacitance with varying scanning rate, the specific capacitance of the cell can be calculated based on CV curves according to equation:

$$C = \frac{Q}{V} = \int \frac{i\ dt}{\Delta V} \quad (1)$$

where *i*, *dt* and $\Delta V$ are the current, the scan time span and the total potential range of the voltage window, respectively. Fig. 4D shows the plots of specific capacitance variations of the cells prepared by using PPy/$MnO_2$/PPF composites as electrode versus scan rate ranging from 10 to 200 mV $s^{-1}$. It can be seen that specific capacitance decreases gradually with the increment of the scan rate, which is attributed to the fact that the doping-undoping

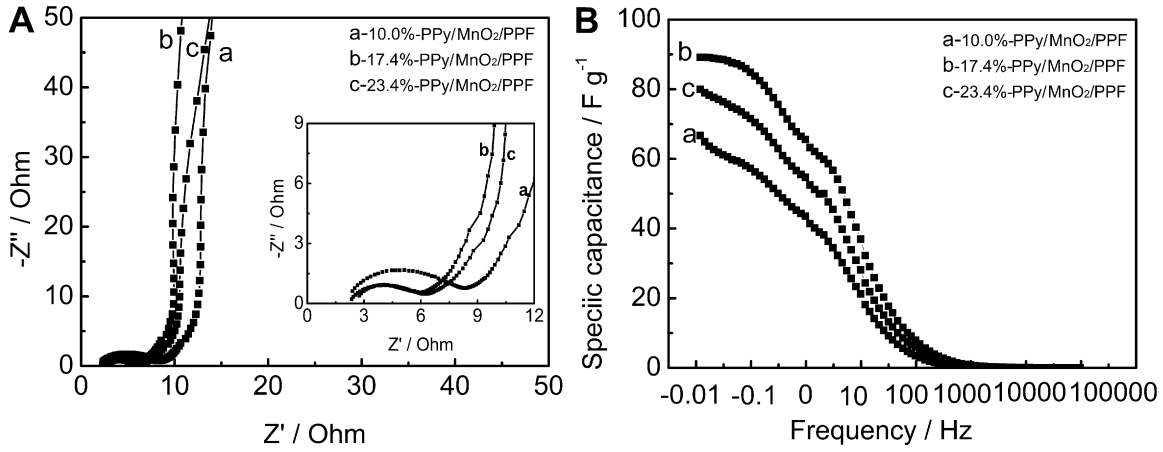


**Fig. 8.** Nyquist plots of the capacitors assembled by PPy/$MnO_2$/PPF composite (A) (insert is the EIS in high-frequency region) and the plots of the specific capacitance of the active material in PPy/$MnO_2$/PPF versus the frequency (B).

reaction in the PPy/$MnO_2$/PPF composite becomes incomplete with the increment of scan rate. Furthermore, it is found that the capacitors assembled by composite b exhibit larger specific capacitance than that assembled by composites a and c.

Fig. 5A shows the charge/discharge curves of the cells prepared by PPy/$MnO_2$/PPF with different amounts of PPy/$MnO_2$ at current density of 1.0 A $g^{-1}$ and the curve b shows longer discharge time than curve a and c, which also indicates that composite b has better capacitance property than composites a and c. Fig. 5B shows the typical galvanostatic charge/discharge curves of the cell assembled by composite b at current densities of 1, 2, 5 and 10 A $g^{-1}$, it is found that the charging curves are very symmetric to their discharging counterparts in the whole potential region, and that the slope of every curve is potential-independent and maintained a constant value during the charging and discharging progress, indicating its excellent behavior of capacitance.

The galvanostatic charge/discharge cycling curves of the cells assembled by PPy/$MnO_2$/PPF composite containing different amounts of PPy/$MnO_2$ at current density of 2 A $g^{-1}$ are shown in Fig. 6, from which it is found that the cells assembled by composite

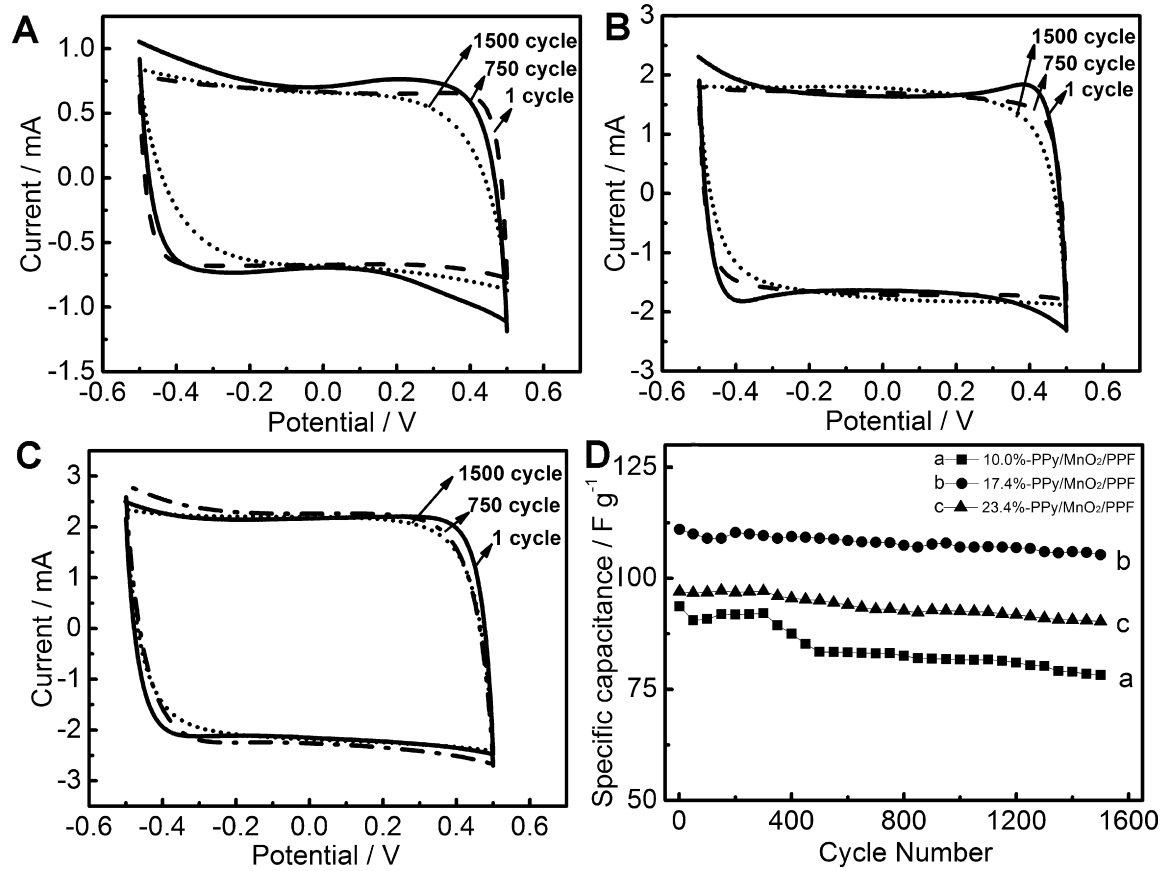


**Fig. 9.** The CV curves of the cells assembled by the composites a (A), b (B) and c (C) under successive CV scan at 50 mV $s^{-1}$, and the relationships between the specific capacitance of the cells and the cycle numbers (D).

b exhibit better stability compared with composites a and c. The discharge capacitance can be calculated from the equation:

$$C_m = \frac{I\ \Delta t}{\Delta V m} \quad (2)$$

where $C_m$, $I$, $\Delta t$, $\Delta V$ and $m$ are the specific capacitance, charge/discharge current, discharge time, the potential window and the mass of active material in the cell, respectively. From the specific capacitance shown in Fig. 7, it can be seen that the specific capacitance decreases slightly when the discharge current increases for all the cells assembled by the composites, but the cell assembled by composite b shows slighter decrement than that assembled by composites a and c.

EIS, as a useful experimental tool to characterize the frequency response of the electrochemical capacitor, can provide the electronic/ionic conductivity of the electrode materials during the charging/discharging progress. All the spectra are expected to exhibit a semicircle in the high frequency region and a linear portion at low frequency region. The interception of the semicircle at the real axis in the high frequency region represents the internal resistance related to the intrinsic electrical resistance of the active materials since the conditions of measurement are kept the same [45]. Fig. 8A represents the Nyquist plots of the capacitor cells determined at open circuit potentials. As pointed out before, a single semicircle in the high-frequency region and a straight line in the low-frequency region are observed. From the inserted plots, it is found that the charge-transfer resistance of the cell assembled by PPy/$MnO_2$/PPF composite b is the smallest, which is an important factor in the fast redox systems such as electrochemical capacitor. In the low frequency, the straight lines almost parallel with imaginary axis for all the cells assembled by PPy/$MnO_2$/PPF, especially those by composite b are observed, indicating that the composite exhibits an ideal capacitive behavior. For electrochemical capacitors, the majority of their capacitance is only available at low frequency, so attention should be paid to the data in this range [46]. Fig. 8B presents the capacitance obtained from EIS for the capacitor assembled by the composites based on the following equation [47]:

$$C_m = \frac{-1}{2\pi m f Z''} \quad (3)$$

Here, $C_m$ is the specific capacitance, $f$ the frequency, $Z''$ the imaginary part of EIS and $m$ the mass of active material in the cell. The capacitance of all the capacitors decreases with the increase of the frequency and behaves like a pure resistance in high frequency region, which reveals that the electrolyte ions cannot be doped/undoped in the matrix of polymer. It is also found that composite b exhibits a higher specific capacitance at low frequency range compared with composites a and c, which is consistent with the results obtained from CV and charge/discharge data. It should be noted that the specific capacitances values of the capacitor cells at 0.01 Hz are deviated from those derived form CV and charge/discharge test, which is mainly due to the different testing systems applied.

As the service life is a very important factor for the electrochemical capacitors' electrodes, so the stability of the cells assembled by the composite has been evaluated by using CV method at a scan rate of 50 mV $s^{-1}$ and the results shown are in Fig. 9. It can be found that the rectangular shapes of the CV curves are almost maintained despite the diminution of specific capacitance with the continuous charge/discharge processes reaches up to 1500 cycles. Furthermore, the specific capacitance of the cells prepared by composites a, b and c retains 83%, 94% and 92% of the initial capacitance, respectively. The 94% specific capacitance retention over 1500 CV cycles can illustrate that the composite b exhibits good stability and may be developed as a suitable material for electrochemical capacitors applications.

## 4. Conclusions

The composites of PPy/$MnO_2$/PPF with various contents of $MnO_2$ have been synthesized successfully in situ by chemical oxidation polymerization in the pyrrole vapor. And the presented PPy/$MnO_2$/PPF composite is lightweight, flexible and mechanically robust electrode material. The specific capacitance of the cells assembled by the optimum PPy/$MnO_2$/PPF is approximately 110 F $g^{-1}$ based on the active material. The electrochemical measurements also show that the capacitors prepared by the optimum composites possess excellent charge/discharge properties at high scanning rate. These types of composite materials may be applied in flexible energy storage devices.

## Acknowledgements

The authors thank the National Natural Science Foundation of China (Grant Nos. 21073115 and 20604014), Natural Science Foundation (2007021008) of Shanxi Province, the Program for New Century Excellent Talents in University (NCET-10-0926) of China and the Program for the Top Young and Middle-aged Innovative Talents of Higher Learning Institutions of Shanxi Province (TYMIT and TYAL).

## References

[1] J.R. McDonough, J.W. Choi, Y. Yang, F.L. Manita, Y.G. Zhang, Y. Cui, Appl. Phys. Lett. 95 (2009) 243109.
[2] P. Chen, G. Shen, S. Sukcharoenchoke, C. Zhou, Appl. Phys. Lett. 94 (2009) 043113.
[3] U.C. Chung, C. Elissalde, S. Mornet, M. Maglione, C. Estournes, Appl. Phys. Lett. 94 (2009) 072903.
[4] X.L. Wu, L.Y. Jiang, F.F. Cao, Y.G. Guo, L.J. Wan, Adv. Mater. 21 (2009) 2710.
[5] W. Sun, X. Chen, J. Power Sources 193 (2009) 924.
[6] Y. Zhang, H. Li, L. Pan, T. Lu, Z. Sun, J. Electroanal. Chem. 634 (2009) 68.
[7] D. Kalpana, K.S. Omukumar, S.S. Kumar, N.G. Renganathan, Electrochim. Acta 52 (2006) 1309.
[8] P. Simon, Y. Gogotsi, Nat. Mater. 7 (2008) 845.
[9] P.J. Hall, M. Mirzaeian, S.I. Fletcher, F.B. Sillars, A.J.R. Rennie, G.O. Shitta-Bey, G. Wilson, A. Cruden, R. Carter, Energy Environ. Sci. 3 (2010) 1238.
[10] K.H. An, W.S. Kim, Y.S. Park, J.M. Moon, D.J. Bae, S.C. Lim, Y.S. Lee, Y.H. Lee, Adv. Funct. Mater. 11 (2001) 387.
[11] D.W. Wang, F. Li, M. Liu, G.Q. Lu, H.M. Cheng, Angew. Chem. Int. Ed. 47 (2007) 373.
[12] H. Zhang, G.P. Cao, Z.Y. Wang, Y.S. Yang, Z.J. Shi, Z.N. Gu, Electrochem. Commun. 10 (2008) 1056.
[13] L.B. Kong, J.W. Lang, M. Liu, Y.C. Luo, L. Kang, J. Power Sources 194 (2009) 1194.
[14] X. Zhang, S.K. Manohar, J. Am. Chem. Soc 126 (2004) 12714.
[15] S. Barman, F. Deng, R.L. McCreery, J. Am. Chem. Soc 130 (2008) 11073.
[16] L.L. Norman, A. Badia, J. Am. Chem. Soc. 131 (2009) 2328.
[17] H.Y. Qin, Z.X. Liu, W.X. Yin, J.K. Zhu, Z.P. Li, J. Power Sources 185 (2008) 909.
[18] G.Y. Han, G.Q. Shi, Thin Solid Films 515 (2007) 6986.
[19] G.Y. Han, G.Q. Shi, J. Appl. Polym. Sci. 103 (2007) 1490.
[20] G.Y. Han, G.Q. Shi, J. Electroanal. Chem. 569 (2004) 169.
[21] T.J. Yao, Q. Lin, K. Zhang, D.F. Zhao, H. Lv, J.H. Zhang, B. Yang, J. Colloid Inter. Sci. 315 (2007) 434.
[22] S.S. Najar, A. Kaynak, R.C. Foitzik, Synth. Met. 157 (2007) 1.
[23] A. Harlin, P. Nousiainen, A. Puolakka, J. Pelto, J. Sarlin, J. Mater. Sci. 40 (2005) 5365.
[24] B.L. He, Y.K. Zhou, W.J. Zhou, B. Dong, H.L. Li, Mater. Sci. Eng. A 374 (2004) 322.
[25] H. Jong-In, Y. In-Hyeong, P. Woon-Kie, J. Electrochem. Soc. 148 (2001) A156.
[26] L.M. Huang, T.C. Wen, A. Gopalan, Electrochim. Acta 51 (2006) 3469.
[27] R.Y. Song, J.H. Park, S.R. Sivakkumar, S.H. Kim, J.M. Ko, D.Y. Park, S.M. Jo, D.Y. Kim, J. Power Sources 166 (2007) 297.
[28] A. Mohammadi, O. Inganas, I. Lundstrom, J. Electrochem. Soc. 133 (1986) 947.
[29] D. Naegele, R. Bittihn, Solid State Ionics 28–30 (1988) 983.
[30] J.Y. Lee, L.H. Ong, G.K. Chuah, J. Appl. Electrochem. 22 (1992) 738.
[31] A. Rudge, J. Davey, I. Raistrick, S. Gottesfeld, J.P. Ferraris, J. Power Sources 47 (1994) 89.
[32] C. Arbizzani, M. Mastragostino, L. Meneghello, Electrochim. Acta 41 (1996) 21.
[33] J.G. Killian, B.M. Coffey, F. Gao, T.O. Poehler, P.C. Searson, J. Electrochem. Soc. 143 (1996) 936.
[34] H.K. Song, G.T.R. Palmore, Adv. Mater. 18 (2006) 1764.

[35] B.N. Grgur, M.M. Gvozdenovic, J. Stevanovic, B.Z. Jugovic, V.M. Marinovic, Electrochim. Acta 53 (2008) 4627.
[36] H. Zhang, G. Cao, Z. Wang, Y. Yang, Z. Shi, Z. Gu, Nano Lett. 8 (2008) 2664.
[37] F. Cheng, J. Zhao, W. Song, C. Li, H. Ma, J. Chen, P. Shen, Inorg. Chem. 45 (2006) 2038.
[38] V. Subramanian, H. Zhu, B. Wei, Chem. Phys. Lett. 453 (2008) 242.
[39] X. Yang, W. Tang, Q. Feng, K. Ooi, Cryst. Growth Des. 3 (2003) 409.
[40] D. Zheng, Z. Yin, W. Zhang, X. Tan, S. Sun, Cryst. Growth Des. 6 (2006) 1733.
[41] J. Li, L. Cui, X.G. Zhang, Appl. Surf. Sci. 256 (2010) 4339.
[42] L. Chen, L.J. Sun, F. Luan, Y. Liang, Y. Li, X.X. Liu, J. Power Sources 195 (2010) 3742.
[43] G.R. Mitchell, Polym. Commun. 27 (1986) 346.
[44] C. Saujianya, S. Radhakrishnan, Polymer 42 (2001) 6723.
[45] D.W. Kim, K.A. Noh, J.H. Chun, S.H. Kim, J.M. Ko, Solid State Ionics 144 (2001) 329.
[46] B.P. Bakhmatyuk, B.Y. Venhryn, I.I. Grygorchak, M.M. Micov, J. Power Sources 180 (2008) 890.
[47] K.S. Ryu, Y.G. Kee, K.M. Kim, Y.J. Park, Y.S. Hong, X.L. Wu, M.G. Kang, N.G. Park, R.Y. Song, J.M. Ko, Synth. Met. 153 (2005) 89.